Ceramics International 50 (2024) 27730–27736

Contents lists available at ScienceDirect

Ceramics International

journal homepage: www.elsevier.com/locate/ceramint

Enhanced photoluminescence emission intensity and stability of deep blue-emissive $(Et_3NH)PbBr_3$ perovskite nanocrystals by using metal-organic frameworks

Tayebeh Hemmati [a], Ali Naghipour [a], Reza Sahraei [a,**], Ehsan Soheyli [b,c,*]

[a] Department of Chemistry, Faculty of Science, Ilam University, Ilam 69315-516, Iran
[b] Department of Physics, Faculty of Science, Ilam University, Ilam 69315-516, Iran
[c] Department of Electrical-Electronics Engineering, Abdullah Gul University, Kayseri 38080, Turkiye

ARTICLE INFO

Handling Editor: Dr P. Vincenzini

Keywords:
$(Et_3NH)PbBr_3$ perovskite
Zr-based MOF
Modified UiO-67
Deep blue emission
Stable emission

ABSTRACT

The primary obstacle faced by researchers in the field of luminescent metal-halide perovskites is their inherent instability, prompting a shift in focus towards enhancing the stability of perovskite nanocrystals (PNCs). One of the promising approaches to address this challenge involves the utilization of metal-organic frameworks (MOFs) to fabricate PNCs@MOF composites. The present study reports a facile and low-cost colloidal strategy to prepare $(Et_3NH)PbBr_3$ PNCs followed by their encapsulation within UiO-67 to enhance their photoluminescence (PL) emission stability. The PNCs and modified UiO-67 were prepared separately via simple and efficient ligand-assisted reprecipitation (LARP) and hydrothermal methods, respectively. After modification of the UiO-67, the pore sizes experienced a substantial increase from 1.90 to 28.84 nm which significantly facilitated the localization of PNCs within the porous matrix. Under a full survey of experimental conditions, the resulting $(Et_3NH)PbBr_3$@UiO-67 composite exhibited a bright deep-blue emission at around 410 nm with an emission quantum yield of 52 %. The emission durability of the fabricated PNCs@MOF composites was assessed against temperature and long-time of storage, confirming the superior advantages of MOF even at elevated temperatures of up to 100 °C. The stable and luminous deep-blue emission displayed by the PNCs@MOF composites in this investigation, offers a promising advancement in materials development for optoelectronic applications.

1. Introduction

Different types of materials have been proposed so far, to address the stability issues related to the perovskite nanocrystals (PNCs), such as polymers [1], inorganic matrices including amorphous silica [2], zeolite [3], CaF_2 [4], metal–organic frameworks (MOFs) [5], layered double hydroxide [6], glasses [7,8], natural materials [9], organic molecules [10], and other alternatives. Among them, MOFs stand out as promising compounds for enhancing the stability of PNCs. They are porous compounds composed of inorganic metal centers and organic components integrated by coordination bonds, forming an expansive lattice-like structure that have received considerable research over the past two decades [11]. These crystalline materials possess numerous advantages, including unique chemical functionalities (adsorption/catalysis), valuable physical properties (luminescence/magnetism), high surface area, adjustable porosity, structural diversity, and different coordination geometries [12,13]. Recently, these materials have demonstrated an additional capability to host the nucleation and growth of PNCs inside their pores, enabling the fabrication of PNCs@MOF composites with stable luminescent characteristics [14]. Indeed, it has been demonstrated that utilizing a well-designed integration of the PNCs with MOFs effectively addresses the stability issues associated with PNCs to achieve better operational stability with superior performance in optoelectronic devices [15].

Various techniques exist to fabricate luminescent PNCs@MOFs composites [16] with many of them focusing on fully inorganic PNCs. One approach involves the independent synthesis of these two components, subsequently merging them under suitable condition. Li et al. separately synthesized $CsPbX_3$ (X = Cl, Br, and I) PNCs by a ligand-free strategy and Cu-BDC MOFs. Then, a certain amount of MOFs was added

* Corresponding author. Department of Physics, Faculty of Science, Ilam University, Ilam 69315-516, Iran.
** Corresponding author.
E-mail addresses: r.sahraei@ilam.ac.ir (R. Sahraei), e.soheyli@ilam.ac.ir (E. Soheyli).

https://doi.org/10.1016/j.ceramint.2024.05.070
Received 28 January 2024; Received in revised form 30 April 2024; Accepted 6 May 2024
Available online 7 May 2024

to the PNCs precursor and stirred for 2 min. The composites showed tunable emissions with PL quantum yield (PLQY) up to 18.3 %, stable for a period of 60 days (under atmospheric conditions in the absence of light) [17]. In another report, PNCs were prepared using the hot-injection method and combined with MOF-5, resulting in durable PL emission centered at 517 nm and 653 nm for $CsPbBr_3$ and $CsPbBr_{0.6}I_{2.4}$ PNCs@MOF-5 composites with excellent PLQY of 81 % and 85 %, respectively [18]. Among the hybrids PNCs, significant efforts have been directed toward the exploration of methylammonium (MA) and formamidinium (FA) cations where hybrid metal halide perovskites of $MAPbBr_3$ and $FAPbBr_3$ with strong green emission were prepared [19, 20]. However, ethylammonium (EA) cation presents an alternative avenue, resulting in ethylammonium lead bromide with bluish emission compared to its counterparts. Sapra's group has demonstrated that by adjusting the ratio of organic cations from MA to EA, the bandgap increases due to the presence of larger *A*-site cations. This adjustment led to PLQY of 85 % at 529 nm (MABr:EABr = 1:0) and 5 % at 432 nm (MABr:EABr = 0:1) [21]. Chu et al. have demonstrated the optimistic role of large EA cations in reducing the Pb–Br orbit coupling in inorganic-based bare perovskite PNCs and the subsequent shift of emission color from green to bluish region [22]. They successfully fabricated perovskite films with a bright sky-blue emission at approximately 480 nm and PLQY of 70 %. However, when EA cations were added (up to 100 %) to replace Cs cations in the original perovskite composition, the PLQY dropped significantly to 22.85 % at 466 nm. In another attempt, Mollick et al., utilized metal-organic gels to simultaneously improve the PLQY (up to 53 %) and emission stability for $EAPbBr_3$@metal-organic gels with PL maximum at 436 nm [23]. Therefore, achieving shorter wavelengths of the blue region with a high PLQY record requires further attention.

In the present study, a facile and room temperature ligand-assisted reprecipitation (LARP) technique is successfully employed for the initial preparation of triethylammonium lead bromide ($(Et_3NH)PbBr_3$) PNCs followed by the hydrothermal preparation of modified UiO-67 MOFs. Then, these components are combined under a well-designed method to fabricate PNCs@MOF composites with strong emission. The obtained composites show stable luminescence in the deep-blue region of the visible spectrum around 410 nm. Through comprehensive optimization of experimental parameters, reproducibility and stability of the PL emission are achieved, indicating the potential of these structures for applications in luminescent-based devices such as light emitting diodes, and photodetectors.

2. Experimental section

2.1. Chemicals and materials

N-octylamine (≥99 %), ethyl acetate (99.9 %), N,N-dimethylformamide (DMF, 98 %), ethanol (EtOH, ≥99.9 %), methanol (MeOH, ≥99 %), toluene (>99 %), diethyl ether (>99 %), ammonia) NH_3, 99 %), citric acid (99 %), ammonium nitrate (98 %), and 3-(N,N-dimethylmyristylammonio)- propanesulfonate (SBE-14, 98 %) were purchased from Merck company and used as received. Zirconium tetrachloride ($ZrCl_4$, 99 %), 4,4-biphenyldicarboxylic acid (H_2BPDC, 99 %), triethylamine ($Et_3N \geq 99.5$ %), hydrobromic acid (HBr, 98 %), cetyltrimethylammonium bromide (CTAB, >98 %), oleic acid (OA, 99 %), lead (II) bromide ($PbBr_2$, 99.9 %), were purchased from Sigma-Aldrich Company and used without further purification.

2.2. Preparation of $(Et_3NH)PbBr_3$ PNCs

Preparation of organic $(Et_3)NHBr$ salt: To prepare Et_3NHBr, 0.27 mmol Et_3N (27 ml) and 15 mL MeOH were mixed with 0.23 mmol HBr (26 mL), and stirred for 2 h in an ice bath. The resulting liquid mixture was then evaporated at 60 °C in a vacuum oven. As-synthesized Et_3NHBr salt (appearing as a yellow precipitate) was washed three times with 20 mL diethyl ether and dried in a vacuum oven at 60 °C for 12 h.

Synthesis of PNCs: The synthesis of $(Et_3NH)PbBr_3$ PNCs was carried out using LARP method. Typically, Et_3NHBr (0.09 mmol) and $PbBr_2$ (0.2 mmol) were dissolved in 5 mL of DMF containing 25 μL of n-octylamine and 0.5 mL of oleic acid to prepare a precursor solution. Then, in a separate beaker, 0.01 mmol SBE-14 was added to 2 mL of toluene. This solution was added to the precursor solution at 120 °C, and stirred vigorously for 20 min, resulting in a yellow-colored solution (mother solution). Subsequently, 2 mL of mother solution was rapidly injected into 5 mL of ethyl acetate (antisolvent) under vigorous stirring at room temperature followed by injection of 1 mL of ammonia solution. Finally, the $(Et_3NH)PbBr_3$ PNCs solution was centrifuged at 6000 rpm for 2 min, and the precipitates were dried for further analysis and processing.

2.3. Synthesis of modified UiO-67

The initial UiO-67 and modified UiO-67 were prepared as follow:

Synthesis of UiO-67 free CTAB (UF): Briefly, 1 mmol (0.23 g) of $ZrCl_4$ was mixed with 1 mmol (0.24 g) of H_2BPDC and dissolved in 30 mL of DMF. The resulting solution was transferred to a 100 mL Teflon-lined stainless steel autoclave and subjected to a temperature of 120 °C for a duration of 24 h inside oven. After cooling down to room temperature, UiO-67 precipitates were washed with 20 mL DMF for three times. Finally, the resulting white powder was dried in a vacuum oven at 120 °C for 12 h.

Synthesis of UiO-67 with CTAB as templating agent (UC): 1 mmol (0.23 g) $ZrCl_4$ was mixed with 1 mmol (0.24 g) of H_2BPDC. Next, CTAB was added and all were dissolved in 30 mL of DMF. Then, the solution was transferred to a 100 mL Teflon-lined stainless steel autoclave, and heated at 120 °C for 24 h. After cooling down to room temperature, the resulting UiO-67 was washed with 20 mL of DMF for three times. Finally, the resulting white precipitate dried in a vacuum oven at 120 °C for 12 h.

Synthesis of UiO-67 with CTAB as chelating agent using ammonium nitrate (UN): 1 mmol (0.23 g) of $ZrCl_4$ was mixed with 1 mmol (0.24 g) H_2BPDC, followed by the addition of CTAB and 30 mL of DMF. Then, the mixture was poured inside a 100 mL Teflon-lined stainless steel autoclave to react for 24 h at 120 °C. After cooling down to room temperature, the resulting UiO-67 underwent a thorough washing process with 20 mL of DMF repeated three times. Eventually, the as-synthesized UiO-67 was subjected to an ion-exchange process at 60 °C for 24 h using 1 M ammonium nitrate EtOH/water solution (volume ratio of 1:2) to remove the template. After washing the product with an EtOH/water mixture, it was dried in a vacuum oven at 120 °C for 12 h.

2.4. Synthesis of PNCs@UN composite

In this procedure, a certain amount of UN was weighed and dispersed in 2 mL of the PNCs mother solution, followed by stirring at room temperature for 30 min. After that, 5 mL of ethyl acetate and 1 mL of ammonia solution were injected under vigorous stirring at room temperature. Finally, the PNCs@UN solution was centrifuged at 6000 rpm for 2 min, and the precipitates were collected and dried for further experiments (Fig. 1).

2.5. Characterizations

The Fourier transform infrared spectroscopy (FT-IR), X-ray diffraction (XRD), energy dispersive x-ray spectroscopy (EDX), field emission scanning electron microscopy (FESEM), transmission electron microscopy (TEM), Elemental mapping, photoluminescence (PL), and Ultraviolet–Visible (UV–Vis) measurements were performed via Bruker-Vertex 70, automated Philips X'Pert X-ray diffractometer, Oxford 7538, FESEM TESCAN MIRA3 (15 keV), Philips CM30 electron

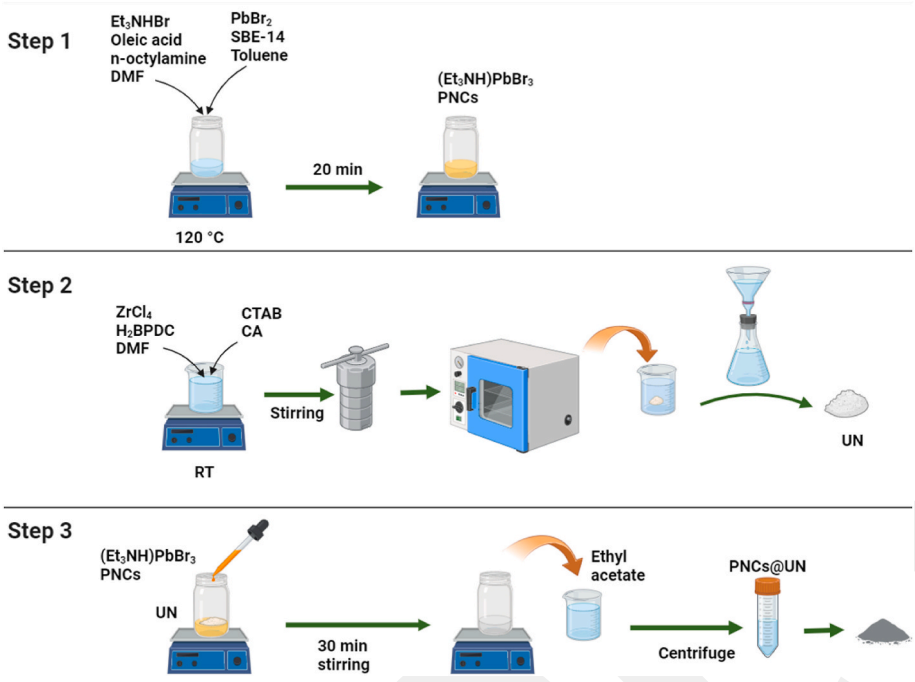

Fig. 1. Schematic diagram of the preparation of PNCs@UN composite.

microscope (operating voltage of 300 kV), Oxford INCA II energy solid-state detector, Cary Eclipse, and Cary 300 Bio instruments, respectively. Nitrogen adsorption and desorption isotherms were measured from the linearity of the Brunauer–Emmett–Teller (BET) calculation, equation.

3. Results and discussion

3.1. Structural analyses

FTIR studies were carried out on UN, PNCs, and PNCs@UN composite as plotted in Fig. 2A. In UN, characteristic peaks at 647-770 cm^{-1}, 1415 cm^{-1}, and 1581 cm^{-1} are assigned to the bending vibrations of benzene rings (C–H), skeletal vibrations of benzene ring (C═C), and coordinated carboxylate groups (COO^{-}), respectively [24]. For PNCs, peaks around 1350-1430 cm^{-1} and 1550-1610 cm^{-1} are assigned to the S═O bonds in SBE-14 and the stretching vibration of COO^{-} of oleic acid, respectively. Additionally, peaks located at 2800-2920 cm^{-1} are attributed to C–H stretching vibrations of oleic acid and SBE-14 [25]. In PNCs@UN composites, peaks around 1350-1430 cm^{-1} and 1550-1610 cm^{-1} are related to the stretching vibrations of the S═O and C═O bonds of the sulfonate (SO_3^{-}) and carboxyl (COOH) groups, respectively. Despite precise drying of the PNCs@UN composite powder, the O–H peak was still observed in the region of 3400–3500 cm^{-1} which indicates the effective presence of H_2BPDC ligand-related O–H groups. XRD measurements further confirmed the synthesis of the PNCs@UN composite. The powder XRD patterns of the prepared samples of PNCs, UN, and PNCs@UN composite are shown in Fig. 2B. The diffraction peaks at 12°, 19.7°, 30.6°, 34.3° and 54° were identified as the diffractions from the (100), (110), (200), (210), and (310) planes of the cubic PNCs [26]. UN exhibited characteristic peaks at 5.6° and 17.1° corresponding to the (111) and (600) lattice planes [27]. The pattern is different from the standard UiO-67 XRD pattern, because we have modified the UiO-67 as already reported elsewhere [28,29]. The XRD pattern of PNCs@UN composite displayed diffraction peaks at 5.6°, 12.6°, 18.1°, 27.3°, 32.7°, and 54.7° assigned to the (111), (100), (600), (200), (210), and (310) lattice planes. These findings suggest that the crystal structure of the PNCs@UN composites retains the UN, proving the successful synthesis of the PNCs@UN composite.

Elemental mapping analysis of the PNCs@UN composites revealed a uniform distribution of the Pb, Zr, Br, O, and C elements within PNCs

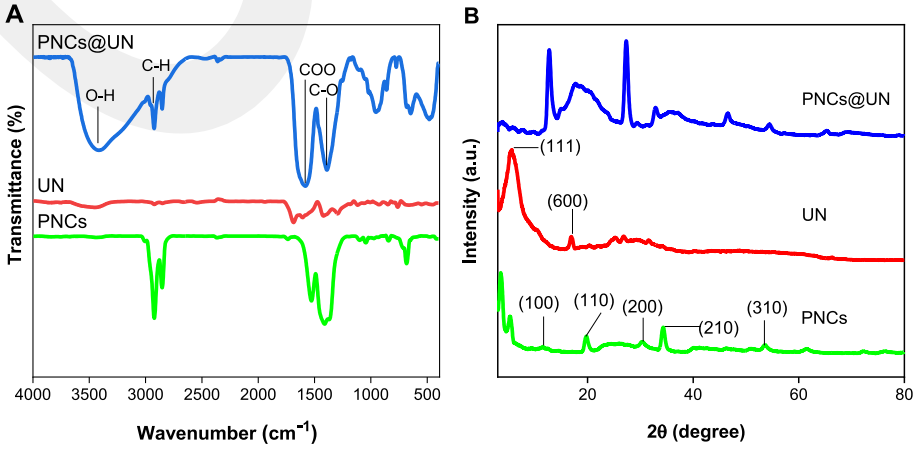

Fig. 2. (A) FTIR spectra of UN, $(Et_3NH)PbBr_3$ PNCs, and PNCs@UN composites. (B) XRD patterns of UN, $(Et_3NH)PbBr_3$ PNCs, and PNCs@UN composites.

and UN (Fig. 3A–E). Additionally, EDX analysis identified characteristic peaks corresponding to Zr, N, C, O, Pb, and Br elements as demonstrated in Fig. 3F. A weak signal of S at around 2.3 eV is related to the SBE-14 ligand consistent with findings from FT-IR results. Fig. 3G and -3H–I showed the FESEM images of UN and PNCs@UN composites at different magnifications, respectively. The TEM images of modified MOF (UN) and bare PNCs were also captured as shown in Fig. 3J–K, respectively. They showed relatively large plate-like structures of UN with sizes of around 150 nm, and tiny PNCs with quasi-spherical shapes typically around 12–18 nm in size.

The porous nature of the UN and PNCs@UN composites was confirmed by BET N_2 adsorption-desorption measurements (Fig. 4). The pore volume and diameter of the UF (as unmodified MOF) were determined to be 0.13 cm^3/g and 1.90 nm, respectively. Upon modification of the UF to UN these values shifted to 0.11 cm^3/g and 28.84 nm, respectively, indicating a significant alteration in pore characteristics. Therefore, with the addition of CTAB and citric acid (UiO-67), the pores size enhanced remarkably and at the same time the pore volume decreased. Citric acid serves as a bridging agent between the positively charged CTAB and the negatively charged carboxylate group of MOF leading to an expansion in pore size after removing CTAB [30]. It facilitated the incorporation of PNCs with dimensions ranging from 12

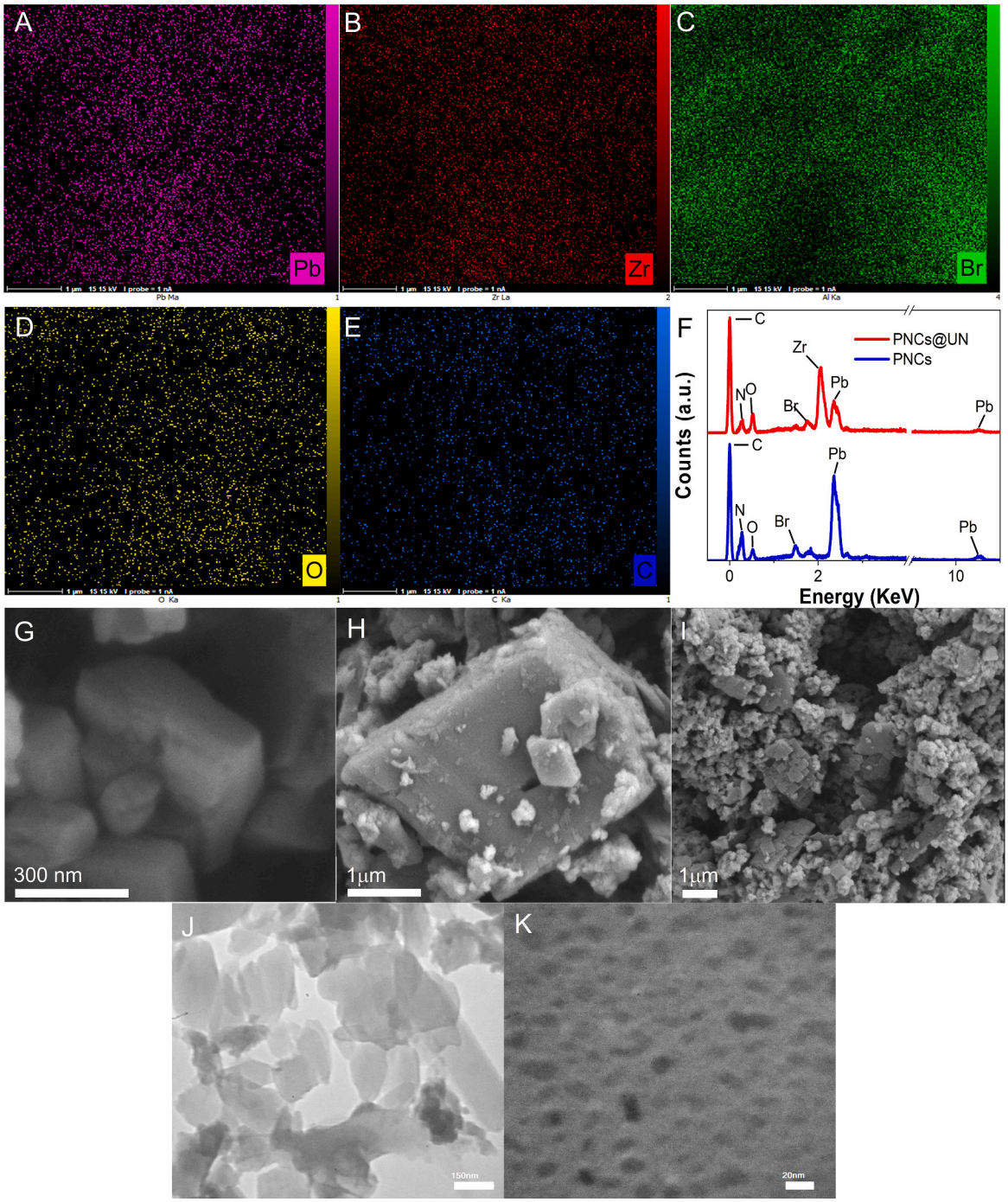

Fig. 3. (A–E) Elemental mapping of Pb, Zr, Br, O, and C elements in PNCs@UN composite. (F) EDX profiles of PNCs and PNCs@UN composites. (G) FESEM image of the prepared UN and (H, I) FESEM images of the fabricated PNCs@UN composites. TEM images of (J) UN (with magnification scale-bar of 150 nm) and (K) PNCs (with magnification scale-bar of 20 nm).

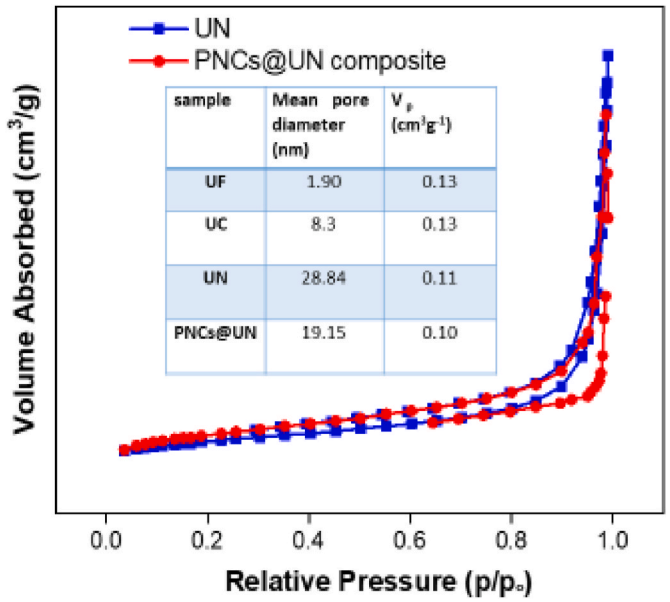

Fig. 4. BET curves of UN and PNCs@UN composites. Insets show a detailed parameters on the pore size, and pore volume of UF, UC, and UN MOF samples along with PNCs@UN composites.

nm to 18 nm into the pores of UN, which were as large as 28.84 nm. Following the fabrication of the composite, the pore volume and diameter in the PNCs@UN composite were measured at 0.10 cm^3/g and 19.15 nm, respectively (as shown in the inset of Fig. 4). Therefore, employing the methodology outlined in this study, the modified UiO-67 works as a better host for PNCs. Also, the pore diameter and volume decreased after the formation of the composite, indicating the successful incorporation of PNCs into the UN pores [13,31].

3.2. Optical analyses

In addition to the structural analyses, which were performed to reveal the morphology and composition of the synthesized samples, optical analyses were also carried out to demonstrate the functionality of these luminescent composites with reproducible properties. Generally, in colloidal-based synthesis approaches of semiconductor nanocrystals, the experimental parameters significantly influence the photophysical characteristics of the prepared samples. In this study, a complete investigation was carried out on the experimental parameters, to achieve optimized results in terms of PL emission in PNCs@UF compositions. The findings are shown in Figs. S1–6. The optimal PNCs@UF composite was achieved under the specified experimental parameters. A combination of 0.09 mmol of Et_3NHBr, 0.2 mmol of $PbBr_2$, and 0.01 mmol of SBE-14 was utilized. Then, 25 μL of n-octylamine, 0.5 mL of oleic acid, and 5 mL of DMF were added to the mixture. Next, 1 mL of this solution was added to 5 mL of ethyl acetate, followed by 20 min of stirring and addition of 2 mL of NH_3. After that, 30 mg of UF was added into 2 mL of PNCs, and quickly injected into 5 mL of ethyl acetate, where it was stirred for 30 min at room temperature. It is noteworthy that our optimization efforts favored UF over UN, because UN is a modified form of UF and all its basic properties depends on the fabrication process and parameters of UF. However, while we specifically optimized with UF, minor optimizations also considered for composite with UN and the final results are shown in Fig. 5. Fig. 5A shows the UV–Vis absorption spectra of $(Et_3NH)PbBr_3$ PNCs, PNCs@UF, PNCs@UC, and PNCs@UN composites within the 300–700 nm wavelengths range. In Fig. 5B, corresponding PL spectra were recorded under excitation at 320 nm. Notably, the absorption edge for all samples was observed at around 400 nm, with the PNCs@UN composite exhibiting lower absorption intensity compared to the others. The PL spectra in Fig. 5B confirms the blue emission of bare PNCs, centered at around 425 nm. Upon formation of the composite using UF and UC, a blue shift was observed in PL emission toward 415 and 410 nm, respectively. Interestingly, the modification to UN (resulting in an increase in the pore-sizes from 1.9 to 28.9 nm), made a notable enhancement in emission intensity with a narrower PL signal centered at 410 nm. The PLQY was measured using comparative method with 9,10-diphenylanthracene as reference dye, given its PL emission signal at 406 and 427 nm, closely matching the PL maxima of prepared PNCs and PNCs@UN samples. Based on the calculations, the fabrication of PNCs@UN composite enhanced the PLQY from 10 % in the case of pristine PNCs to 52 % which is a high record for such a deep-blue emissive hybrid PNCs@MOF composite. After purification, the composites were dissolved in toluene to assess their luminescent properties, as illustrated in Fig. 5C, which demonstrates the preserved intense emission of PNCs, UN, and PNCs@UN composite in the solvent.

3.3. Thermal stability and long-term storage stability of $(Et_3NH)PbBr_3$ PNCs and PNCs@UN composite

To perform thermal stability tests, a certain amount of PNCs and PNCs@UN powders were poured inside glass vials and subjected to a controlled heating process inside a programmable oven. Fig. 6A and B illustrate the thermal stability of the PL spectrum for $(Et_3NH)PbBr_3$ PNCs and PNCs@UN composite, respectively. As the temperature rises from 25 °C to 70 °C, the PL intensity of $(Et_3NH)PbBr_3$ PNCs diminished completely with no emission signal. In contrast, the PL intensity of UN-protected PNCs only decreased to 85 % of the initial value even at 100 °C, highlighting the crucial role of MOF-encapsulation in protecting the bare $(Et_3NH)PbBr_3$ PNCs. The relative PL intensity of both samples was also plotted in Fig. 6C against temperatures. Besides, to evaluate and compare the long-term stability of $(Et_3NH)PbBr_3$ PNCs and PNCs@UN composite, they were stored under laboratory conditions and PL spectra were monitored over a period of 180 days (Fig. 6D and E). The findings validate the enhanced stability of PNCs post-encapsulation with UN, as MOF with bigger pore sizes, as evidenced by the sustained luminescence even after 6 months of storage. The relative PL intensity of both samples was also graphed in Fig. 6F against the storage duration, which confirms the positive impact of MOF encapsulation on the stability of the prepared PNCs.

The fundamental concept revolves around the necessity of localizing PNCs within the meticulously designed pores of MOFs to achieve a stable compound. The critical aspect is ensuring that these two components possess compatible sizes. Therefore, initial UiO-67 (UF) was modified to UN in order to transform UiO-67 MOFs into structures with bigger pore sizes. This modification facilitates the incorporation of PNCs within the UN matrix, with the UN pores serving as a protective barrier for the PNCs that are susceptible to structural deformation and degradation in ambient atmospheric conditions. By preventing the surface of the PNCs from interacting with the external environment, UN enhances the stability of the PNCs and mitigates the risk of PNCs aggregation. Furthermore, UN's reliable chemical stability makes it an ideal template for stabilizing PNCs. At the same time, as a result of facilitated insertion of more PNCs inside UN, the PL intensity and PLQY enhanced remarkably to 52 %.

4. Conclusions

In summary, a simple and versatile two-step strategy was proposed for the fabrication of bright blue-emissive composite of PNCs@UN. The synthesis of PNCs utilized the LARP technique, involving the injection of PNCs precursors and capping ligands into the solvent. Additionally, hydrothermal method was used for the synthesis of UN. Initially, a thorough optimization of experimental parameters was considered to realize the highest emission intensity with reproduced results. The final product of PNCs@UN composite showed improved stability (thermal

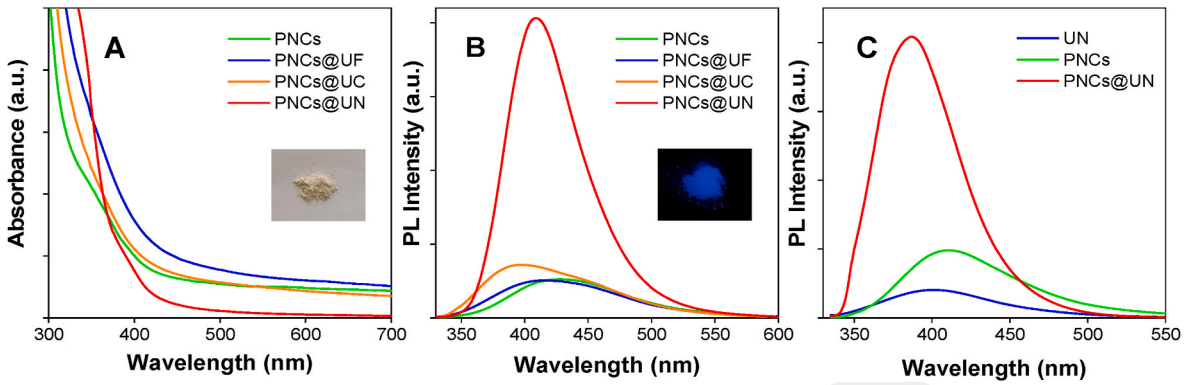

Fig. 5. (A) The UV–Vis absorption of $(Et_3NH)PbBr_3$ PNCs, PNCs@UF, PNCs@UC, and PNCs@UN composites; (B) The PL spectra (λ_{exc} = 320 nm) of PNCs, PNCs@UF, PNCs@UC, and PNCs@UN composites; (C) The PL emission spectra (λ_{exc} = 320 nm) of PNCs, UN, and PNCs@UN composite powders dissolved in toluene.

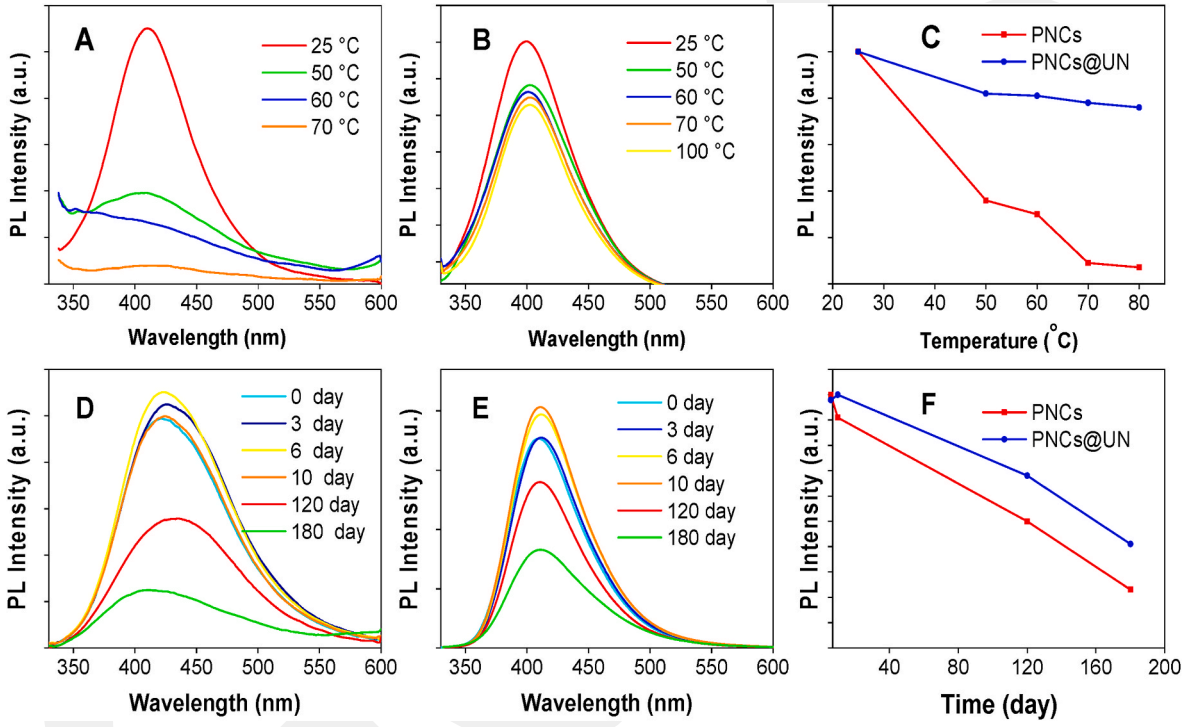

Fig. 6. (A-B) Thermal stability tests of $(Et_3NH)PbBr_3$ PNCs and PNCs@UN composite. (C) The normalized PL intensity evolution of $(Et_3NH)PbBr_3$ PNCs and PNCs@UN composite as a function of temperature. (D-E) Long-term storage stability tests of $(Et_3NH)PbBr_3$ PNCs and PNCs@UN composite. (F) The normalized PL intensity evolution of $(Et_3NH)PbBr_3$ PNCs and PNCs@UN composite as a function of storage time.

stability, long-term stability) along with a notable increase in PLQY compared to the pristine $(Et_3NH)PbBr_3$ PNCs. The composite achieved a remarkable PLQY of 52 % at an emission peak of approximately 410 nm, underscoring the protective role of MOF which propose the fabricated samples for diverse optoelectronic applications.

Data availability statement

The data that support the findings of this study are available from the corresponding author upon reasonable request.

CRediT authorship contribution statement

Tayebeh Hemmati: Formal analysis, Investigation, Writing – original draft. **Ali Naghipour:** Methodology, Project administration, Resources, Supervision, Validation. **Reza Sahraei:** Funding acquisition, Project administration, Resources, Supervision, Writing – review & editing. **Ehsan Soheyli:** Conceptualization, Methodology, Supervision, Validation, Writing – original draft, Writing – review & editing.

Declaration of competing interest

The authors declare that they have no known competing financial interests or personal relationships that could have appeared to influence the work reported in this paper.

Acknowledgements

The authors would like to acknowledge Ilam University for its financial support.

Appendix A. Supplementary data

Supplementary data to this article can be found online at https://doi.

org/10.1016/j.ceramint.2024.05.070.

References

[1] Y. Xin, H. Zhao, J. Zhang, Highly stable and luminescent perovskite–polymer composites from a convenient and universal strategy, ACS Appl. Mater. Interfaces 10 (2018) 4971–4980, https://doi.org/10.1021/acsami.7b16442.

[2] S. Huang, Z. Li, L. Kong, N. Zhu, A. Shan, L. Li, Enhancing the stability of CH3NH3PbBr3 quantum dots by embedding in silica spheres derived from tetramethyl orthosilicate in "waterless" toluene, J. Am. Chem. Soc. 138 (2016) 5749–5752, https://doi.org/10.1021/jacs.5b13101.

[3] T. Shi, X. Chen, Y. Deng, H. Huang, J. Wang, R. He, Y. Liu, X. He, J. Li, P.K. Chu, X.-F. Yu, Scalable synthesis of ultrastable lead halide perovskite-zeolite composites via a chemical vapor method in air, NPG Asia Mater. 14 (2022) 87, https://doi.org/10.1038/s41427-022-00433-0.

[4] Y. Wei, H. Xiao, Z. Xie, S. Liang, S. Liang, X. Cai, S. Huang, A.A. Al Kheraif, H. S. Jang, Z. Cheng, J. Lin, Highly luminescent lead halide perovskite quantum dots in hierarchical CaF2 matrices with enhanced stability as phosphors for white light-emitting diodes, Adv. Opt. Mater. 6 (2018) 1701343, https://doi.org/10.1002/adom.201701343.

[5] S. Mollick, T.N. Mandal, A. Jana, S. Fajal, A. V Desai, S.K. Ghosh, Ultrastable luminescent hybrid bromide perovskite@MOF nanocomposites for the degradation of organic pollutants in water, ACS Appl. Nano Mater. 2 (2019) 1333–1340, https://doi.org/10.1021/acsanm.8b02214.

[6] Y. Liu, B. Shi, Q. Liu, C. Lü, Large-scale synthesis of layered double hydroxide nanosheet-stabilized CsPbBr3 perovskite quantum dots for WLEDs, J. Alloys Compd. 843 (2020) 155819, https://doi.org/10.1016/j.jallcom.2020.155819.

[7] S. Samiei, E. Soheyli, K. Vighnesh, G. Nabiyouni, A.L. Rogach, Exploring CsPbX3 (X = Cl, Br, I) perovskite nanocrystals in amorphous oxide glasses: innovations in fabrication and applications, Small 20 (2024) 2307972, https://doi.org/10.1002/smll.202307972.

[8] B. Yang, S. Mei, Y. Zhu, D. Yang, H. He, R. Hu, Y. Li, J. Zou, R. Guo, Precipitation promotion of highly emissive and stable CsPbX3 (Cl, Br, I) perovskite quantum dots in borosilicate glass with alkaline earth modification, Ceram. Int. 49 (2023) 6720–6728, https://doi.org/10.1016/j.ceramint.2022.10.205.

[9] S. Karabel Ocal, N.B. Kiremitler, A.F. Yazici, N. Celik, E. Mutlugun, M.S. Onses, Natural wax-stabilized perovskite nanocrystals as pen-on-paper inks and doughs, ACS Appl. Nano Mater. 5 (2022) 6201–6212, https://doi.org/10.1021/acsanm.2c00224.

[10] X.-Y. Wang, M.-X. Wu, S.-N. Ding, Anodic electrochemiluminescence from CsPbBr3 perovskite quantum dots for an alkaline phosphatase assay, Chem. Commun. 56 (2020) 8099–8102, https://doi.org/10.1039/D0CC03648J.

[11] M. Safaei, M.M. Foroughi, N. Ebrahimpoor, S. Jahani, A. Omidi, M. Khatami, A review on metal-organic frameworks: synthesis and applications, TrAC Trends Anal. Chem. 118 (2019) 401–425, https://doi.org/10.1016/j.trac.2019.06.007.

[12] W. Wang, D. Wang, H. Song, D. Hao, B. Xu, J. Ren, M. Wang, C. Dai, Y. Wang, W. Liu, Size effect of gold nanoparticles in bimetallic ZIF catalysts for enhanced photo-redox reactions, Chem. Eng. J. 455 (2023) 140909, https://doi.org/10.1016/j.cej.2022.140909.

[13] J. Ren, A. Meijerink, X. Zhou, J. Wu, G. Zhang, Y. Wang, In situ embedding synthesis of CsPbBr3@Ce-MOF@SiO2 nanocomposites for high efficiency light-emitting diodes: suppressing reabsorption losses through the waveguiding effect, ACS Appl. Mater. Interfaces 14 (2022) 3176–3188, https://doi.org/10.1021/acsami.1c20804.

[14] H. Shankar, S. Ghosh, P. Kar, Boosting the stability of lead halide perovskite nanocrystals by metal–organic frameworks and their applications, J. Mater. Chem. C 10 (2022) 11532–11554, https://doi.org/10.1039/D2TC02243E.

[15] S.K. Yadav, G.K. Grandhi, D.P. Dubal, J.C. de Mello, M. Otyepka, R. Zbořil, R. A. Fischer, K. Jayaramulu, Metal halide Perovskite@Metal-organic framework hybrids: synthesis, design, properties, and applications, Small 16 (2020) 2004891, https://doi.org/10.1002/smll.202004891.

[16] J. Hou, Z. Wang, P. Chen, V. Chen, A.K. Cheetham, L. Wang, Intermarriage of halide perovskites and metal-organic framework crystals, Angew. Chemie - Int. Ed. 59 (2020) 19434–19449, https://doi.org/10.1002/anie.202006956.

[17] Z. Li, C. Yu, Y. Wen, Z. Wei, J. Chu, X. Xing, X. Zhang, M. Hu, M. He, MOF-confined sub-2 nm stable CsPbX3 perovskite quantum dots, Nanomaterials 9 (2019) 1147, https://doi.org/10.3390/nano9081147.

[18] J. Ren, T. Li, X. Zhou, X. Dong, A.V. Shorokhov, M.B. Semenov, V.D. Krevchik, Y. Wang, Encapsulating all-inorganic perovskite quantum dots into mesoporous metal organic frameworks with significantly enhanced stability for optoelectronic applications, Chem. Eng. J. 358 (2019) 30–39, https://doi.org/10.1016/j.cej.2018.09.149.

[19] K. Oh, K. Jung, D. Park, M.-J. Lee, Highly luminescent CH3NH3PbBr3 quantum dots with 96.5% photoluminescence quantum yield achieved by synergistic combination of single-crystal precursor and capping ligand optimization, J. Alloys Compd. 859 (2021) 157842, https://doi.org/10.1016/j.jallcom.2020.157842.

[20] Y. Zu, J. Xi, L. Li, J. Dai, S. Wang, F. Yun, B. Jiao, H. Dong, X. Hou, Z. Wu, High-brightness and color-tunable FAPbBr3 perovskite nanocrystals 2.0 enable ultrapure green luminescence for achieving recommendation 2020 displays, ACS Appl. Mater. Interfaces 12 (2020) 2835–2841, https://doi.org/10.1021/acsami.9b18140.

[21] M. Mittal, A. Jana, S. Sarkar, P. Mahadevan, S. Sapra, Size of the organic cation tunes the band gap of colloidal organolead bromide perovskite nanocrystals, J. Phys. Chem. Lett. 7 (2016) 3270–3277, https://doi.org/10.1021/acs.jpclett.6b01406.

[22] Z. Chu, Y. Zhao, F. Ma, C.-X. Zhang, H. Deng, F. Gao, Q. Ye, J. Meng, Z. Yin, X. Zhang, J. You, Large cation ethylammonium incorporated perovskite for efficient and spectra stable blue light-emitting diodes, Nat. Commun. 11 (2020) 4165, https://doi.org/10.1038/s41467-020-17943-6.

[23] S. Mollick, T.N. Mandal, A. Jana, S. Fajal, S.K. Ghosh, A hybrid blue perovskite@metal-organic gel (MOG) nanocomposite: simultaneous improvement of luminescence and stability, Chem. Sci. 10 (2019) 10524–10530, https://doi.org/10.1039/C9SC03829A.

[24] D. Zhang, J. Zhao, Q. Liu, Z. Xia, Synthesis and luminescence properties of CsPbX3@Uio-67 composites toward stable photoluminescence convertors, Inorg. Chem. 58 (2019) 1690–1696, https://doi.org/10.1021/acs.inorgchem.8b03295.

[25] G.-Y. Qiao, D. Guan, S. Yuan, H. Rao, X. Chen, J.-A. Wang, J.-S. Qin, J.-J. Xu, J. Yu, Perovskite quantum dots encapsulated in a mesoporous metal–organic framework as synergistic photocathode materials, J. Am. Chem. Soc. 143 (2021) 14253–14260, https://doi.org/10.1021/jacs.1c05907.

[26] R.K. Singh, R. Kumar, A. Kumar, N. Jain, R.K. Singh, J. Singh, Novel synthesis process of methyl ammonium bromide and effect of particle size on structural, optical and thermodynamic behavior of CH3NH3PbBr3 organometallic perovskite light harvester, J. Alloys Compd. 743 (2018) 728–736, https://doi.org/10.1016/j.jallcom.2018.01.355.

[27] X.-Q. Zhan, F.-C. Tsai, L. Xie, K.-D. Zhang, H.-L. Liu, N. Ma, D. Shi, T. Jiang, Ligands-coordinated Zr-based MOF for wastewater treatment, Nanomaterials 8 (2018) 655, https://doi.org/10.3390/nano8090655.

[28] L.-J. Zhong, B. Jiang, K. Tang, Efficient resolution of 4-chlormandelic acid enantiomers using lipase@UiO-67(Zr) zirconium-organic frameworks in organic solvent, Chirality 35 (2023) 323–333, https://doi.org/10.1002/chir.23542.

[29] K. Wang, W. Zhao, Q. Zhang, H. Li, F. Zhang, In situ one-step synthesis of platinum nanoparticles supported on metal–organic frameworks as an effective and stable catalyst for selective hydrogenation of 5-hydroxymethylfurfural, ACS Omega 5 (2020) 16183–16188, https://doi.org/10.1021/acsomega.0c01759.

[30] G. Cai, P. Yan, L. Zhang, H.-C. Zhou, H.-L. Jiang, Metal–organic framework-based hierarchically porous materials: synthesis and applications, Chem. Rev. 121 (2021) 12278–12326, https://doi.org/10.1021/acs.chemrev.1c00243.

[31] H.-Y. Guan, R.J. LeBlanc, S.-Y. Xie, Y. Yue, Recent progress in the syntheses of mesoporous metal–organic framework materials, Coord. Chem. Rev. 369 (2018) 76–90, https://doi.org/10.1016/j.ccr.2018.05.001.